Supplementary Information

A Comparative Investigation of the Sorption of Polycyclic Aromatic Hydrocarbons to Various Polydisperse Micro- and Nanoplastics using a Novel Third-Phase Partition Method

Emeka Ephraim Emecheta[1,2], Diana Borda Borda[1], Patrizia Marie Pfohl[3], Wendel Wohlleben[3], Christoph Hutzler[1], Andrea Haase[1*], Alexander Roloff[1*]

[1]German Federal Institute for Risk Assessment, Department of Chemical and Product Safety, Berlin, Germany

[2]University of Bayreuth, Bayreuth Center for Ecology and Environmental Research (BayCEER), Bayreuth, Germany

[3]BASF SE, Carl-Bosch-Str. 38, 67056 Ludwigshafen, Germany

Corresponding authors:

Alexander Roloff, alexander.roloff@bfr.bund.de

Andrea Haase, andrea.haase@bfr.bund.de

Number of pages 30

Number of figures 7

Number of tables 7

Table of Content

Section S1: Quality Control / Quality Assurance 3

Figure S1: Examples of TD-GC-MS calibration curves for PAHs: 5

Table S1: Physical-chemical properties of polymers investigated in this study. 6

Table S2: Experimental conditions for the sorption isotherm experiments of PAHs and MNPs.. 7

Section S2: Determination of sorption kinetics and partition coefficients of PAHs for polydimethylsiloxane and water ($K_{PDMS/W}$) 8

Figure S2: [a] First-order one-compartment model fit of experimental data (n = 2, mean ± SD) of PDMS sorption kinetics. 12

Section S3: Determination of kinetics of PAH sorption on MNPs in water. 12

Table S3: Parameters of pseudo-first and pseudo-second order kinetics models. 13

Figure S3: Verification of B[a]P sorption equilibrium for selected MNP variants 13

Section S4: Sorption Isotherms and Model Fittings. 14

Figure S4: Exemplary experimental isotherms (n = 3, mean ± standard deviation) of PAHs: (a) Anth, (b) B[a]P and (c) DB[a,l]P adsorptions to PA-6_42 fitted to different adsorption isotherm models. 18

Table S4: Isotherm model fit parameters for PAH adsorption to PA-6_42. 18

Section S5: Validation of the modified third-phase partition method: Batch-equilibrium method for determination of adsorption isotherms for PAHs and MNPs in water. 19

Table S5: Comparison of the logarithmic adsorption coefficient $K_{MNP,W}$ (L/kg) acquired applying the batch-equilibrium and TPP methods (n = 5 isotherm points in duplicate or triplicate, mean ± SD). 22

Figure S5: Verification of equilibrium for the adsorption of B[a]P on (a) PA-6, (b) LDPE, and Anth on (c) PA-6 and (d) LDPE MNPs. 23

Figure S6: Comparison of the Langmuir adsorption isotherms of (a) B[a]P and (b) Anth adsorption to LDPE_215 and PA-6_42 MNPs acquired with the TPP method and the batch-equilibrium method. 23

Section S6: Experimentally Determined PAH Sorption Coefficients $K_{MNP/W}$ and Associated Combined Measurement Uncertainties 24

Table S6: Experimentally determined sorption coefficients of PAHs onto MNPs obtained using the TPP method. 26

Table S7: contributions of the uncertainty components of $K_{MNP/w}$ for the PAHs 27

Section S7: Evaluation of competitive sorption: sorption behavior of MNPs in single and tri-sorbate systems. 27

Figure S7: Langmuir coefficient K_L of the adsorption of Anth, B[a]P and DB[a,i]P on (a) LDPE_215 and (b) PA-6_42 MNPs in single and tri-adsorbate systems. 28

References SI 29

Section S1: Quality Control / Quality Assurance

Desorption efficiencies of the PDMS-coated stir-bars were evaluated by performing a carryover test. Desorbed stir-bars were desorbed a second time after purging the TD-GC-MS system via a blank run with empty thermal desorption (TD) tubes. Desorption efficiencies were calculated as the peak areas of the respective PAH signal from the first desorption divided by the peak areas of the first and second desorption multiplied with 100. For Anth and B[*a*]P as well as their respective internal standards, the obtained desorption efficiencies were > 99%. DB[*a,l*]P and DB[*a,i*]P yielded similar desorption efficiency in the range of 85–90%.

To minimize variability and cross-contamination, the TD-GC-MS system was always cleaned by running pre-conditioned empty TD tubes in between every sample. The optimized TDU method utilized for the purging was 720°C/min; held for 5 min. The cold injection system (CIS) was operated in split mode at a high flow of 700 mL/min and a split ratio of 700:1 and held for 5 min at 320°C. The transfer temperature from TDU to CIS was 350°C. The GC oven was operated at a temperature of 60°C for 0.5 min; heated to 300°C at 40°C/min; and then to 320°C at 35°C/min and held for 5 min.

The PDMS-coated magnetic stir-bars were conditioned for re-use by drenching them in acetonitrile overnight or methylene chloride/methanol (50:50, *v*/*v*) for 2 h. Afterwards, the stir-bars were removed from the solvent and baked out under nitrogen flow (100 mL/min) at 300°C for at least 2 h in a TDU conditioner from Gerstel. Used TD glass tubes were also heated out alongside the stir-bars to recondition them for re-use. After the TDU conditioner was turned off, the stir-bars and TD glass tubes were allowed to cool to at least 50°C, and stored inside a clean beaker that was covered with aluminum foil before further use.

Glass vials utilized for incubation were prepared for re-use by washing them in a dishwasher, followed by rinsing with milli-Q water and heating out in an oven at 150°C for 30 mins.

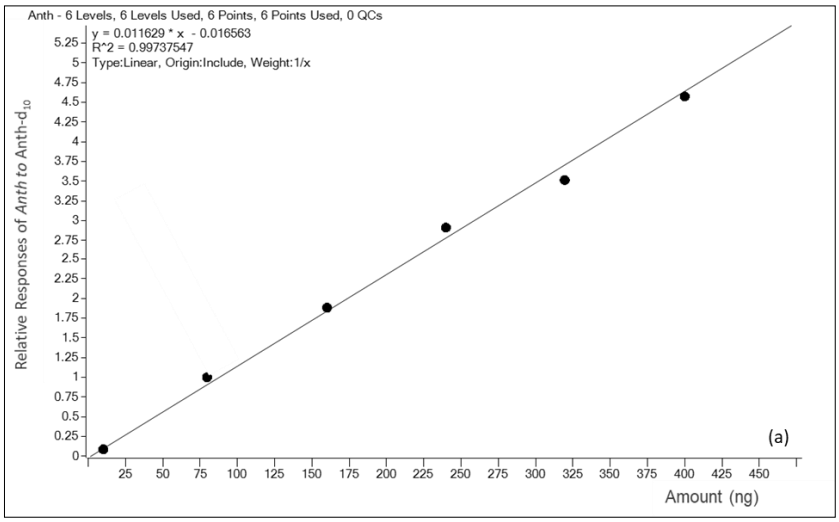

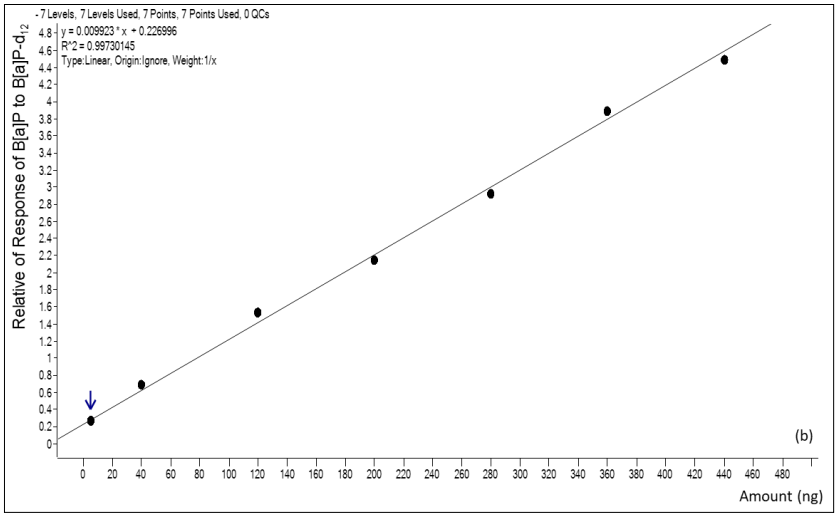

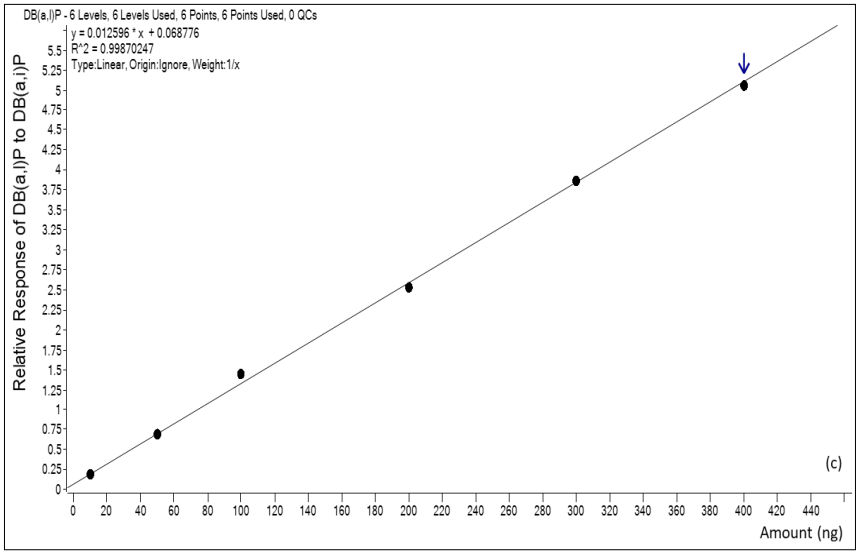

Figure S1: Examples of TD-GC-MS calibration curves for PAHs: (a) Anth, (b) B[a]P and (c) DB[a,l]P. The limit of detection (LOD) was estimated with the MassHunter software as the concentration corresponding to 3 × signal to noise ratio. The limit of quantification (LOQ) was calculated as 3×LOD. The mean LOD (n=6) for Anth, B[a]P and DB[a,l]P was 0.5, 0.8 and 1.2 ng, respectively.

Table S1: Physical-chemical properties of polymers investigated in this study.

Name	Variants	Size Distribution (µm)			T_m (°C)	BET S.A (m^2/g)	T_g (°C)	Crystallinity	Density (g/ml)	Supplier
		Dx10	Dx50	Dx90						
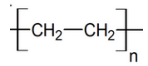 **LDPE**	LDPE_215	96,2	215,5	380,0	104	0,243	-27	Semicrystalline	0.917	BASF SE
	LDPE_84	19,1	84,4	188,0	104	0,326	-27	Semicrystalline	0.917	BASF SE
	PE_0.6	0,3	0,6	1,9	n.a.	n.a.	-80, -120 [b]	Semicrystalline	0.95 - 0.98	BASF SE
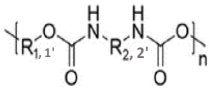 **TPUs**	ester_arom	142,0	254,0	418,0	169	0,027	-40	Amorphous	1.12	BASF SE
	ester_alip	143,0	262,0	440,0	159	0,035	-50	Amorphous	~ 1.2	BASF SE
	ether_arom	128,0	246,0	413,0	169	0,030	-37	Amorphous	-1.12	BASF SE
	ether_alip	152,0	267,0	442,0	159	0,033	-10	Amorphous	~ 1.2	BASF SE
	melt_arom	272,0	864,0	1560,0	52	n.a.	-49	Amorphous	1.12-1.2	BASF SE
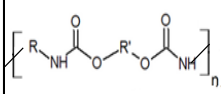 **PUs**	PU_foam	33,1	92,8	211,0	n.a.	1,183	n.a.	Amorphous	1 - 1.2	BASF SE
	arom_1C	82,8	200,0	354,0	n.a.	0,145	n.a.	Amorphous (cross-linked)	~ 1.2	BASF SE
	arom_2C	77,2	201,0	368,0	n.a.	0,159	31	Amorphous (cross-linked)	~ 1.2	BASF SE
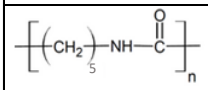 **PA-6**	PA-6_7	2,3	6,9	13,5	220	1,850	53	Semicrystalline	1 -1.2	BASF SE
	PA-6_42	13,7	42,2	75,3	220	0,366	53	Semicrystalline	1 -1.2	BASF SE
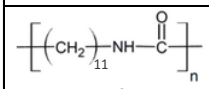 **PA-12**	PA-12_44	34,4	44,3	57,0	177	0,726	38	n.a.	n.a.	BASF SE
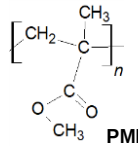 **PMMA**	PMMA_0.3	0,3	0,3	0,4	>160	15,000	44, 105[b]	n.a.	~ 1	BASF SE
	PMMA_6	2,2	6,2	11,6	>160	1,619	44, 105[b]	n.a.	~ 1	BASF SE
Tire Rubber 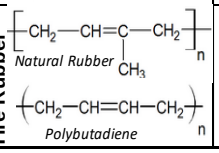 *Natural Rubber* *Polybutadiene*	Tire Rubber	61,7	130,0	233,0	n.a.	0,298	-60 °C		1,19	BASF SE

Data from suppliers unless otherwise stated.

[b] Chemical Retrieval on the Web (CROW), 2021, polymerdatabase.com.

T_m = Melting point temperature. T_g = Glass transition temperature. BET S.A = Brunauer–Emmett–Teller surface area.

n. a. = not available

Table S2: Experimental conditions for the sorption isotherm experiments of PAHs and MNPs. A volume of 240 mL water was used for all sorption experiments.

Isotherm experiments	Conc. range (ng/L)	Mass of MNPs (mg)	Incubation time (h)	Isotherm points	Replicate per isotherm point
LDPE_215 + 3-PAH Mix	0 - 2500	5,0	104	7	3
PA-6_42 + 3-PAH Mix	0 - 3000	2,5	72	7	3
LDPE_215 + DB*[a,L]*P	0 - 2000	5,0	110	7	2
PA-6_42 + DB*[a,L]*P	0 - 2000	2,5	62	7	2
TPU_ester_arom + DB*[a,L]*P	0 - 2000	5,0	100	7	3
LDPE_215 + ANT	0 - 2000	5,0	62	7	3
PA-6_42 + ANT	0 - 3000	2,5	15	7	3
TPU_ester_arom + ANT	0 - 3000	10,0	34	5	3
LDPE_215 + B*[a]*P	0 - 3750	5,0	108	7	2
PA-6_42 + B*[a]*P	0 - 3750	2,5	36	7	3
TPU_ester_arom + B*[a]*P	0 - 4000	5,0	64	7	3
TPU_ester_alip + B*[a]*P	0 - 4000	5,0	66	7	3
TPU_ether_arom + B*[a]*P	0 - 4000	5,0	117	7	3
TPU_ether_alip + B*[a]*P	0 - 4000	5,0	66	6	2
TPU_ melt_ arom + B*[a]*P	0 - 4000	5,0	106	6	2
PU foam + B*[a]*P	0 - 3750	5,0	108	7	3
PU_arom_1C + B*[a]*P	0 - 3750	5,0	92	7	3
PMMA_0.3 + B*[a]*P	0 - 3750	8,0	92,5	7	3
PMMA_6 + B*[a]*P	0 - 3750	8,0	95,5	7	3
PU_arom_2C + B*[a]*P	0 - 3750	10,0	88	7	3
Tire Rubber + B*[a]*P	0 - 4500	3,0	72	6	3
PA-6_7 + B*[a]*P	0 - 3750	2,5	70	7	2
PA-12_44 + B*[a]*P	0 - 4000	5,0	86	6	3
LDPE_84 + B*[a]*P	0 - 3750	5,0	72	5	2
PE_0.6 + B*[a]*P	0 - 5000	4,0	72	6	2
Tire Rubber_1000h aged + B[a]P	0 - 5000	5,0	76	6	2
PA-6_42_1000h aged + B[a]P	0 - 5000	3,0	68	6	2
LDPE_215_1000h aged + B[a]P	0 - 5000	5,0	96	6	2
Tire Rubber_2000h aged + B[a]P	0 - 5000	5,0	68	5	3
PA-6_42_2000h aged + B[a]P	0 - 5000	3,0	72	5	3
LDPE_215_2000h aged + B[a]P	0 - 5000	5,0	76	5	3

Section S2: Determination of sorption kinetics and partition coefficients of PAHs for polydimethylsiloxane and water ($K_{PDMS/w}$)

Prior to the kinetics experiments, the stability and recovery of the PAHs were determined via control experiments in 6 replicates. 1 µg/L PAHs were incubated in 240 mL water (without MNPs and PDMS) for 48 h, extracted and quantified following the conditions described below. Average recoveries of 95–120% for Anth, 80–130% for B[*a*]P and 64–67% for DB[*a,l*]P were obtained.

In order to obtain $K_{PDMS/w}$, the equilibrium time for the sorption of the PAHs onto the PDMS passive samplers was determined via kinetics experiments. For all experiments, PDMS-coated stir-bars of 24 µL PDMS phase volume were incubated in 240 mL water spiked with 1 µg/L of target PAHs. Multipoint stirring plates operating at 600 rotations per minute (rpm) were used for all incubations inside a temperature-controlled chamber which was operated at 21°C. The sorption kinetics of Anth and B[*a*]P were evaluated in duplicate. At specified time intervals, replicate vials were withdrawn from the stirring plate, the PDMS-coated stir-bars inside the vials were removed with clean tweezers and wiped gently on a lint-free tissue. 100 ng of the respective internal standard (Anth-d_{10} for Anth, B[*a*]P-d_{12} for B[*a*]P) were spiked on the surface of the PDMS-coated stir-bars, which were held with tweezers until the solvent was fully evaporated. The loaded stir bars were inserted inside pre-conditioned empty TD glass tubes, which were subsequently capped with transport adapters. The amount of PAHs sorbed to the passive samplers at each time point were quantified via TD-GC-MS as described in the method section of the manuscript.

As shown in **Figure S2a**, the experimentally determined sorption kinetics of the PAHs were fitted to the first-order one-compartment model using **Equation S1** [1]:

$$C_{PDMS}(t) = C_{W,O}\ \frac{k_1}{k_2}\ (1 - e^{-k_2 t}) \qquad \textbf{Equation S1},$$

where k_1 and k_2 are the uptake and release rate constants, respectively. $C_{PDMS}(t)$ (µg/kg) and $C_{w,0}$ (µg/L) are the sorbed analyte concentration at time t and the initial analyte concentration in the aqueous phase, respectively.

Using the release rate constants k_2 from the above equation, the time required to reach 90% of equilibrium t_{90} can be estimated by ln (10/k_2) [2]. This resulted in t_{90} values of 32 and 76 h for Anth and B[a]P, respectively. Notably, the obtained equilibrium times are similar to the findings of Prieto et al. [3] who utilized similar PDMS-coated stir-bars. Thus, the values of $K_{PDMS/w}$ for Anth and B[*a*]P were determined after 66 and 136 h of incubation respectively, which were beyond the t_{90} equilibration time.

With knowledge of the equilibration time, $K_{PDMS/w}$ of the PAHs were determined for five concentration levels. Each concentration level was evaluated in duplicate. PDMS-coated stir-bars of 24 µL PDMS-phase volume were utilized for all $K_{PDMS/w}$ experiments. The samples were stirred on a stirring plate inside an incubation chamber until t_{90} was reached. Experiments were conducted at concentrations below the solubility limit of the respective PAHs but sufficiently high to quantify the aqueous phase concentration at t_{90} [4]. For Anth (water solubility: 44 µg/L) [5, 6], $K_{PDMS/w}$ was determined at different initial concentrations up to 1750 ng/L in 240 mL water. Regarding the more hydrophobic B[*a*]P (water solubility: 2–4 µg/L) [5, 6], initial concentrations up to 1700 ng/L in 3.5 L water were used. This ensured that up to two-thirds of the total amount of B[*a*]P in the system remained in the aqueous phase after 136 h of incubation, which was well beyond t_{90}. The concentration of PAHs that partitioned to the PDMS phase (C_{PDMS})

were quantified via TD-GC-MS whereas the PAH concentration remaining in the aqueous phase (C_w) was determined via a stir-bar sorptive extraction (SBSE) process [3, 7, 8]. Therefore, 100 ng of the respective internal standard was spike into the solution, which was subsequently extracted with a PDMS-coated stir-bar (126 µL PDMS phase volume) for 48 h. Following SBSE, the PAH-load on the PDMS-coated stir-bar was analyzed via TD-GC-MS.

Mass balance for the super-hydrophobic DB[*a,l*]P could not be achieved. This is presumably due to its extremely low water solubility, which can cause losses of analyte through precipitation and/or adsorption of significant fractions to surfaces. The log of $K_{PDMS/w}$ was calculated using a linear relation of log $K_{PDMS/w}$ and the logarithmic octanol/water partition coefficient log $K_{o/w}$ derived for super-hydrophobic (log $K_{o/w} > 4$) pollutants according to **Equation S2** [9]:

$$K_{PDMS/w} = 1.16 \log K_{o/w} - 2.06 \qquad \textbf{Equation S2}.$$

Mass balance of Anth and B[*a*]P were successfully evaluated across the investigated concentration ranges by comparing the sum of PAHs extracted from the aqueous and PDMS phases with the initial amount of PAHs. This revealed a good recovery of 102 ± 10% and 92 ± 12% for Anth and B[*a*]P, respectively. $K_{PDMS/w}$ (L/kg) for Anth and B[*a*]P was subsequently calculated as the ratio of PAH concentrations partitioned onto the PDMS-coated stir-bar and water (**Equation S3**):

$$K_{PDMS/w} = \frac{C_{PDMS}}{C_w} \qquad \textbf{Equation S3},$$

where C_{PDMS} (µg/kg) and C_w (µg/L) are the concentrations of PAHs in the PDMS and water phases, respectively.

As shown in **Figure S2b**, the values for $K_{PDMS/w}$ for Anth and B[*a*]P were 11421 ± 2255 L/kg and 141244 ± 37444 L/kg respectively; or 4.05 ± 0.09, and 5.13 ± 0.10 in log scale

192 for Anth and B[*a*]P, respectively. The PDMS-water partition coefficients determined
193 herein for Anth and B[*a*]P were consistent with previous values as reviewed by
194 DiFilippo et al [10].

195 It is noteworthy that to qualify as a third-phase polymer, it is favorable that sorption of
196 POPs (PAHs) to the polymer, in this case the PDMS coating of the stir bar, occurs via
197 'true-partitioning' [11, 12]. True partitioning is often confirmed by (1) microscopy [12], (2)
198 by a linear relationship between the partition coefficient $K_{\text{third-phase/water}}$ of the POP
199 bewteen the third-phase polymer and water and $K_{o/w}$ [9], (3) by sorption kinetics
200 following a first-order one-compartment model and (4) by linear sorption isotherms
201 over a wide concentration range [11].

202 Mayer et al. [12] have demonstrated PAH partitioning into PDMS coatings. Notably, an
203 important reason for adopting PDMS as a third-phase polymer in this study is the wide
204 linear range of the dependency of $K_{\text{PDMS/w}}$ on $K_{o/w}$ for POPs (with a slope close to unity
205 stretching up to log $K_{o/w}$ = 7.51 [12]), which compares favorably to other third-phase
206 polymers such as polyoxymethylene (POM) [11]. The log $K_{o/w}$ of PAHs studied herein
207 ranged from 4.45 to 7.71. Furthermore, the linearity of the sorption isotherms for
208 partitioning to PDMS (**Figure S2b**) as well as a good fit of the first-order one-
209 compartment model to the partitioning kinetics data (**Figure S2a**), together with the
210 above-mentioned points informed our choice of PDMS as passive sampler in this
211 study.

212

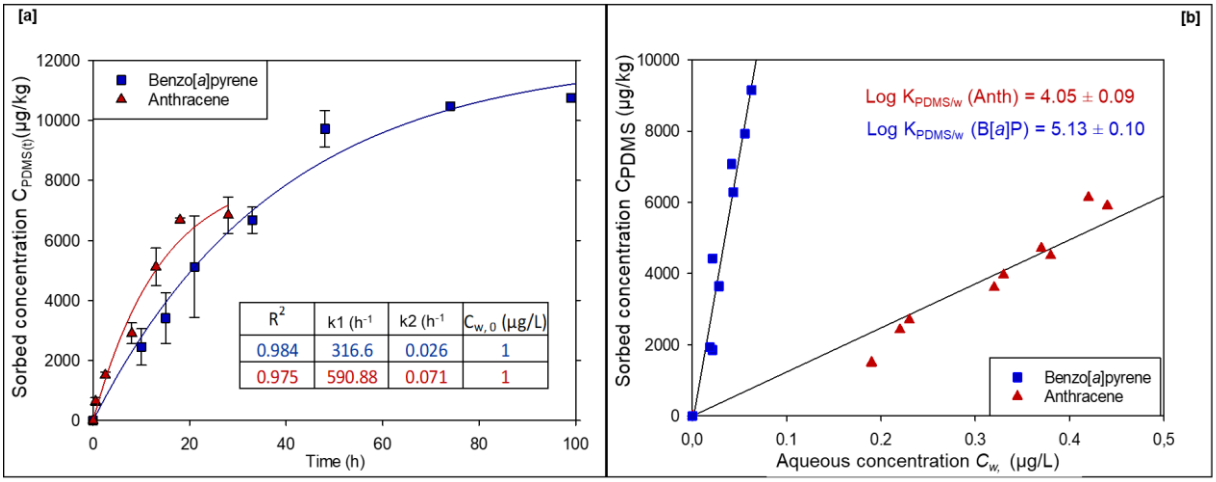

Figure S2: [a] First-order one-compartment model fit of experimental data (n = 2, mean ± SD) of PDMS sorption kinetics and [b] sorption isotherms and corresponding partition coefficients (derived from the slopes of linear regressions) of PAHs and PDMS in water.

Section S3: Determination of kinetics of PAH sorption on MNPs in water.

The parameters of pseudo-first and -second order models are shown in **Table S3**. As indicated, both models were compared utilizing their respective coefficients of determination (R^2) and the chi-square errors (χ^2) to evaluate their performance. For the three PAHs, R^2 of the pseudo-second order fittings were generally slightly better than for the pseudo-first order model (**Table S3**). However, a two-tailed student t-test analysis ($p \leq 0.05$) of the calculated $C_{MNP,t}$ from both models as well as their goodness of fit values (R^2, χ^2) indicated no significant difference. Also, the initial adsorption rates h which are equal to $k_b q_e^2$ show that the sorption of the PAHs onto the MNPs are relatively high in the beginning.

For B[*a*]P, pivot kinetics experiments were performed for three MNPs: PA-6, LDPE and Tire Rubber that were aged under UV-exposure for 1000 h, as well as variants of (T)PU MNPs. As shown in **Figure S3**, equilibrium was verified by a comparison of B[*a*]P adsorption onto the MNPs in the near-equilibrium region of the sorption processes using a fixed concentration of 1 µg/L. Equilibrium verification was indirectly obtained via a comparison of the PAH concentrations of the resulting aqueous phases following

the separation of MNPs via filtration after incubation at two time intervals within the equilibrium region. There were no significant differences for various different MNPs, suggesting that sorption equilibrium has been reached.

Table S3: Parameters of pseudo-first and pseudo-second order kinetics models.

Adsorbate	Adsorbent	Pseudo-first order				Pseudo-second order			
		k_a (h^{-1})	q_e (µg/g)	R^2	χ^2 (µg/g)	k_b (g µ$g^{-1}h^{-1}$)	h (µg $g^{-1}h^{-1}$)	R^2	χ^2 (µg/g)
Anth	PA-6_42µm	0,281	10,0	0,929	2,11	0,048	5,51	0,950	1,39
	LDPE_215µm	0,096	17,0	0,973	1,30	0,006	2,34	0,973	0,94
	TPU_ester_arom	0,092	13,8	0,981	0,31	0,005	1,56	0,963	0,63
B[a]P	PA-6_42µm	0,178	25,0	0,920	5,98	0,009	6,57	0,893	8,06
	LDPE_215µm	0,079	18,3	0,983	0,54	0,004	1,98	0,986	0,93
	PMMA_6µm	0,076	9,4	0,961	1,00	0,009	1,03	0,976	0,60
	Tire Rubber	0,098	35,01	0,988	1,50	0,003	4,92	0,977	3,81
	PU_arom_1C	0,145	11,59	0,985	0,77	0,015	2,5	0,992	0,35
	TPU_ester_arom	0,114	42,58	0,965	5,56	0,003	7,44	0,982	2,82
DB[a,*L*]P	PA-6_42µm	0,135	19,24	0,933	4,29	0,011	4,70	0,944	3,12
	LDPE_215µm	0,272	38,85	0,936	8,91	0,018	34,86	0,998	0,09
	TPU_ester_arom	0,211	8,22	0,945	0,54	0,037	2,93	0,960	0,34

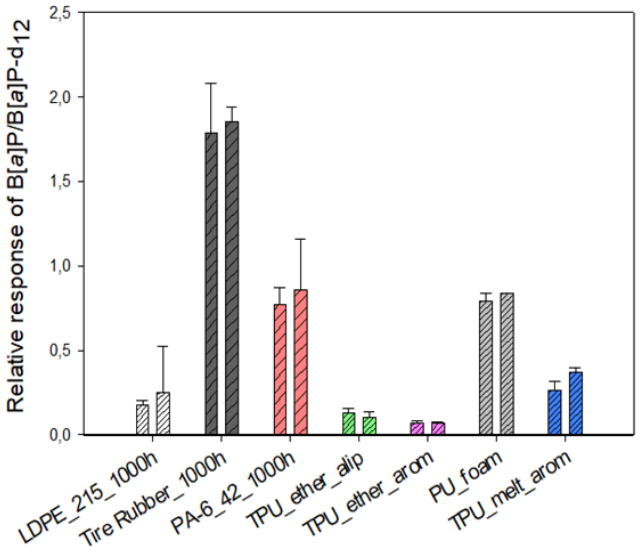

Figure S3: Verification of B[a]P sorption equilibrium for selected MNP variants (LDPE_215_1000h, PA-6_42_1000h and Tire Rubber_1000h MNPs were compared at 72 and 100 h, TPU_ether_alip and TPU_ether_arom MNPs were both evaluated at 62 and 106 h, TPU_melt_arom and PU_foam MNPs were assessed at 108 and 132 h, bars represent the average of duplicate measurement at the specified time intervals, error bars indicate ±SD).

Section S4: Sorption Isotherms and Model Fittings.

In order to obtain some mechanistic insight into the sorption of PAHs onto MNPs, sorption isotherms were evaluated by applying eight different isotherm models (**Figure S4**). In addition to the parameter of the models, R^2 and χ^2 were utilized to compare the models. R^2 values close to 1 and low values of χ^2 indicate good fits. The parameters and error functions of the isotherm model fittings of B[*a*]P sorption to PA-6_42 MNPs are exemplified in **Table S4.**

If the isotherm is linear across the tested concentration range, it typically fits to the Henry model [13], a one-parameter model which describes the sorption behavior of the sorbent at low concentration of the sorbate (**Equation S4**). K_H (L/kg) is the Henry isotherm constant.

$$C_{MNP} = K_H C_w \qquad \textbf{Equation S4}.$$

The Dubinin-Radushkevich (Dub-Rad) model [14] which assumes a pore filling sorption mechanism with a Gaussian energy distribution onto heterogonous surfaces is commonly applied to distinguish between chemisorption and physisorption using its mean free energy *E* which is equal to $1/\sqrt{(2K_{ad})}$. K_{ad} (mol^2/ kJ^2) is the isotherm constant while ε and q_s (µg/g) are the Dub-Rad constant and the theoretical maximum sorption capacity, respectively (**Equation S5**).

The calculated mean free energy values for the sorption of PAHs to MNPs in water from this study range from 41–75 kJ/mol. A number of studies [15-17] investigating sorption isotherms of pollutants have suggested that mean free energy values > 8 kJ/mol imply that sorption involves partitioning into the bulk. Consequently, we

conclude that partitioning is significantly contributing to the sorption of PAHs to MNPs studied herein.

$$C_{MNP} = q_S * (e^{-K_{ad}*\varepsilon^2}) \quad \textbf{Equation S5}.$$

Unlike other models, the Tempkin model contains a factor which describes sorbent/sorbate interactions b_T (**Equation S6**). It assumes that the heat of adsorption of moleules decreases linearly rather than logarithmically with an increase in surface coverage [18]. However, it ignores extremely low and large concentration values (**see Figure S4**). A_T (L/kg) is the Tempkin adsorption constant.

$$C_{MNP} = \frac{RT}{b_T} * \ln A_T\, C_w \quad \textbf{Equation S6}.$$

The Freundlich model includes possible heterogeneities between the adsorption sites at the adsorbent surface [19]. K_F (L/kg) and n are the Freundlich isotherm coefficient and exponent respectively (**Equation S7**).

$$C_{MNP} = K_F * C_w \text{^} n \quad \textbf{Equation S7}.$$

The Brunauer-Emmett-Teller (BET) model (**Equation S8**) theoretically describes multilayer adsorption systems in the gas phase [20, 21], but it has also been modified and widely applied for liquid-solid adsorptions [21]. K_S (L/µg) is the isotherm constant which corresponds to α_L (L/µg) for a single layer adsorption. q_m (µg/g) is the monolayer adsorption capacity while K_l (L/µg) is the equilibrium constant for adsorption at upper layers. The poor fit of this model to our isotherms suggest monolayer adsorption.

$$C_{MNP} = q_m \frac{Ks * C_w}{(1 - K_l * C_w)(1 - K_l * C_w + Ks * Cw)}$$ **Equation S8**.

Sips (**Equation S9**) and Redlich-Peterson (Red-Pet, **Equation S10**) models are 3-parameter empirical models. The former aims to circumvent the limitation of the Freundlich isotherm, according to which the concentration of the adsorbate increases infinitely for surfaces with finite adsorption sites. The latter is widely used as a compromise between Langmuir and Freundlich systems. The goodness of fit parameters for both models were better than those for the two-parameter models. This is unsurprising because both models contain three adjustable parameters. However, the parameters obtained from these models were inconsistent with those obtained from the Freundlich and Langmuir models. This is probably due to the additional errors induced by additional parameterization of the models. K_R (L/kg) and K_{sip} (L/kg) are the Red-Pet and Sips isotherm constants, respectively. n is the dimensionless exponent while α_R (L/µg) and α_L (L/µg) are constants related to the activation energy for Red-Pet and Sips, respectively.

$$C_{MNP} = \frac{\mathrm{K_{sip}}\, C_W{}^{n}}{1 + \alpha_S\, C_W{}^{n}}$$ **Equation S9**,

$$C_{MNP} = \frac{\mathrm{K}_R\, C_W}{1 + \alpha_R\, C_W{}^{n}}$$ **Equation S10**.

The Langmuir model describes monolayer adsorption. It assumes that adsorption can only occur at a finite number of definite localized sites and is characterized by a plateau – an equilibrium saturation point, where once a molecule occupies a site, no further adsorption can occur [22]. It is most commonly used to quantify and contrast different

bio-sorbents [19]. From all tested 2-parameter models, the Langmuir model resulted in the best fitting across the tested concentration ranges and thus was chosen to compare the adsorption of PAHs to all investigated MNPs (**Table 2**). K_L (L/kg) is the Langmuir adsorption coefficient and equals $\alpha_L * q_{max}$. α_L (L/µg) is the Langmuir isotherm constant which is related to the free energy of adsorption [23], while q_{max} (µg/kg) is the theoretical maximum monolayer adsorption capacity (**Equation S11**). In addition to the Langmuir parameters, the Langmuir equilibrium factor $R_L = 1 / (1+ \alpha_L\ q_o)$ [23] was utilized to compare the adsorption isotherms. Here, α_L is the Langmuir constant (L/mg), and q_o is the initial concentration of adsorbent (mg/L).

$$C_{MNP} = \frac{K_L * C_w}{1 + \alpha_L * C_w} \qquad \textbf{Equation S11}.$$

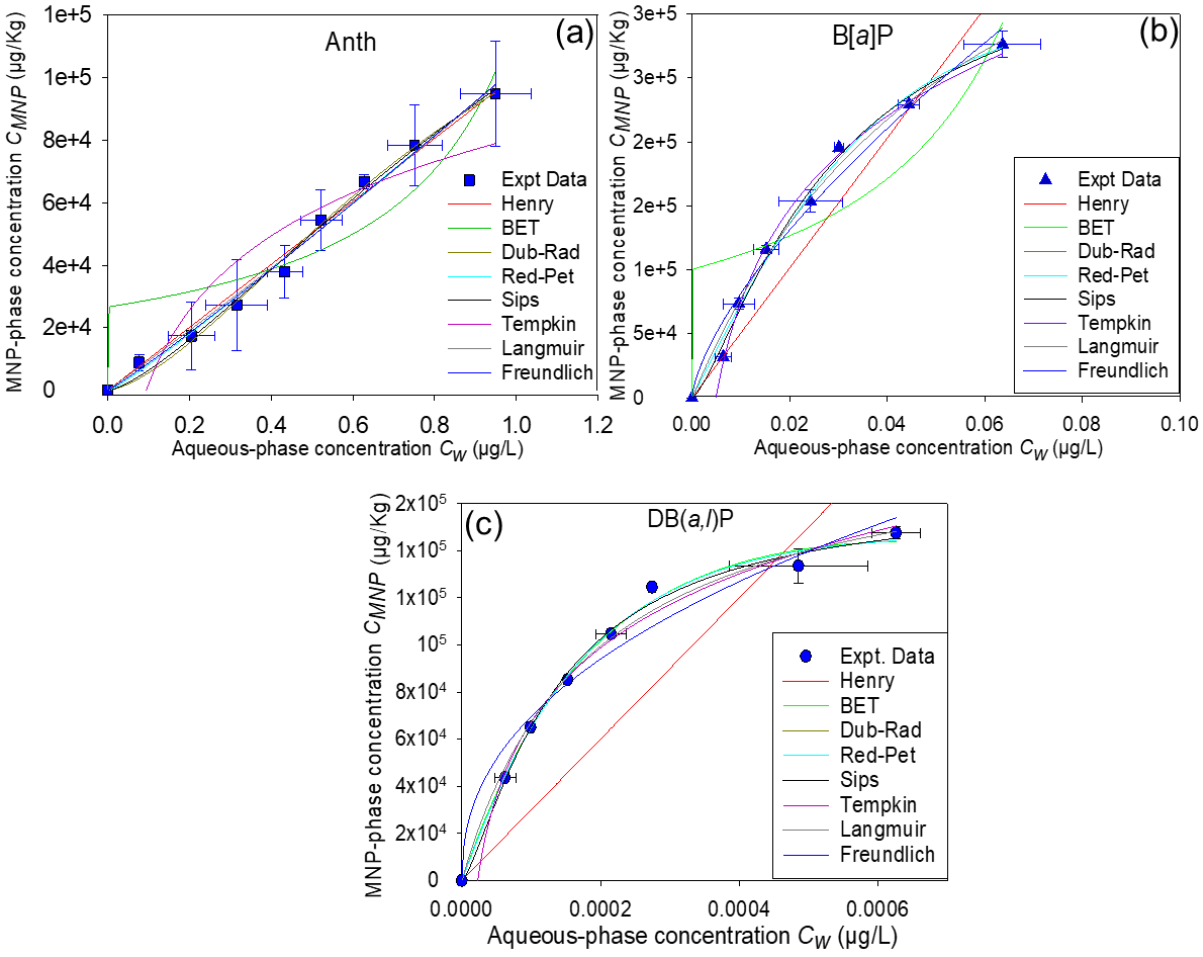

Figure S4: Exemplary experimental isotherms (n = 3, mean ± standard deviation) of PAHs: (a) Anth, (b) B[a]P and (c) DB[a,l]P adsorptions to PA-6_42 fitted to different adsorption isotherm models.

Table S4: Isotherm model fit parameters for PAH adsorption to PA-6_42.

Models	PAHs	Model parameters			Error functions	
		K_L (Log)	**q_{max} (µg/g)**		**R^2**	**χ^2 [µg/g]**
Langmuir	Anth	5.04	1136		0.989	4.5
	B[*a*]P	6.96	540		0.990	14.3
	DB[*a,l*]P	9.01	192		0.991	1.6
		K_F (Log)	**n_F**		**R^2**	**χ^2 [µg/g]**
Freundlich	Anth	5.00	0.95		0.989	4.03
	B[*a*]P	6.28	0.68		0.976	28.75
	DB[*a,l*]P	6.57	0.43		0.966	7.56
		A_T (L kg^{-1})	**b_T**		**R^2**	**χ^2 [µg/g]**
Tempkin	Anth	12.05	0.07		0.904	56.11
	B[*a*]P	204	0.02		0.995	2.56
	DB[*a,l*]P	44231	0.05		0.989	1.60
		K_{ad} (mol^2/ kJ^2)	**q_s (µg/g)**	**E (kJ/mol)**	**R^2**	**χ^2 [µg/g]**
Dub-Rad	Anth	0.0003	149	41	0.993	4.32
	B[*a*]P	0.0001	1897	71	0.976	1437.53
	DB[*a,l*]P	0.0001	3735	75	0.966	7.56
		K_H (Log)			**R^2**	**χ^2 [µg/g]**
Henry	Anth	5.01			0.990	12.92
	B[*a*]P	6.71			0.891	44.76
	DB[*a,l*]P	8.48			0.509	93.43
		K_s (L/µg)	**K_l (L/µg)**	**q_m (µg/g)**	**R^2**	**χ^2 [µg/g]**
BET	Anth	813790891	0.76	28227	0.871	63.70
	B[*a*]P	9741894726	10	100546	0.815	222
	DB[*a,l*]P	417	-1286	2059729	0.994	0.79
		K_{sip} (Log)	**n**	**α_s (L/µg)**	**R^2**	**χ^2 [µg/g]**
Sips	Anth	5.01	0.96	0.03	0.989	5.25
	B[*a*]P	7.65	1.35	123.4	0.994	5.10
	DB[*a,l*]P	10.39	1.34	149662	0.995	0.76
		K_R (Log)	**n**	**α_R (L/µg)**	**R^2**	**χ^2 [µg/g]**
Red-Pet	Anth	5.02	8.02	0.08	0.991	4.22
	B[*a*]P	6.88	1.59	63.03	0.992	9.36
	DB[*a,l*]P	8.90	1.30	36358	0.995	0.73

Section S5: Validation of the modified third-phase partition method: Batch-equilibrium method for determination of adsorption isotherms for PAHs and MNPs in water.

The novel third-phase partition method was verified using the batch-equilibrium method commonly applied to determine sorption isotherms [24]. For two sorbates (Anth and B[a]P) and two MNP sorbents (LDPE_215 and PA-6_42) sorption isotherms were acquired using the two methods and the obtained adsorption coefficients were compared.

Regarding the batch-equilibrium experiment, B[*a*]P sorption kinetic and isotherm experiments were performed in 500 mL Duran glass vials while those of Anth were conducted in 250 mL Duran glass vials. 5 mg of the target MNPs were utilized for all experiments except for characterizing B[*a*]P sorption onto PA-6_42, where 2.5 mg was used. Shaking of the sample vials were conducted in a two-dimensional IKA® HS 250 compact orbital shaker operated at 200 rpm and positioned inside a temperature-controlled incubation chamber (Binder GmbH, Tuttlingen, Germany). The samples were incubated at 21 ± 1^{o}C until the predetermined minimum equilibrium time was reached. After shaking, the sample vials were filtrated. Owing to the high initial rate of Anth sorption by PA-6_42, internal standard was spiked into the supernatant after filtration in order to circumvent sorption of Anth-d_{10} by the PA-6_42 particles. For B[*a*]P and LDPE_215, internal standard was spiked into the sample mixtures right before filtration. This corrects for the significant losses of B[*a*]P due to binding of this analyte to the filter material. Filtration was performed quickly (< 10 mins) without vacuum. After filtrations, the filtrates were extracted with 2×60 mL (Anth) or 2×100 mL (B[*a*]P) hexane. The combined organic extracts where dried over 3–6 g of anhydrous sodium sulfate,

and subsequently concentrated to < 0.1 mL using a BUCHI R-215 Rotavapor System at a vacuum pump pressure of 260 mbar and a water bath temperature of 50^{o}C. Final volumes of 100 µL (B[*a*]P) and 500 µL for (Anth) were constituted with hexane and transferred to GC-vials. For quantification, 1 µL of the sample extracts were injected into a GC-MS system operated in splitless mode of the cold injection system (CIS). The method for GC-MS and data analysis were the same as described for the TPP method.

The minimum equilibrium times for sorption were predetermined by incubating the respective MNPs using a fixed B[*a*]P concentration of 1.0 µg/L in duplicate for different time intervals ranging from 36–336 h. Equilibrium was assumed when the difference between the average aqueous phase sorbate concentration for two consecutive time points are within the respective standard deviations.

The isotherm experiments were conducted at five different initial PAH concentrations, and were measured at least in duplicate. Initial Anth concentrations of 0.75, 1.50, 2.25, 3.00, 3.50 µg/L in 240 mL water and initial B[*a*]P concentrations of 0.5, 1.0, 1.5, 2.0, 2.5 µg/L in 500 mL water were utilized.

For quality control, triplicates of two concentration points (lowest and highest) were used as control samples (PAH + water) and blank samples (water + MNPs) and were subjected to same conditions as the test samples.

Like the TPP method, an isotherm plot of the aqueous phase concentration of the analyte C_W (µg/L) vs the concentration of analyte sorbed to the MNP phase C_{MNP} (µg/kg) was fitted to the Langmuir model. C_W and C_{MNP} were calculated from **Equation S12** and **S13**, respectively. The sorption coefficient $K_{MNP/w}$ (L/kg) was calculated as the ratio of C_{MNP} and $C_{w.}$

$$C_W = \frac{n}{V_W}$$ **Equation S12**,

$$\mathrm{C_{MNP}} = \mathrm{C_0} - \mathrm{C_W}$$ **Equation S13**,

where V_w (L), C_0 (µg/L) and n (µg) are the volume of water, the initial adsorbate concentration and the measured amount of the sorbate, respectively.

Under the experimental conditions utilized, minimum equilibrium times for the sorption of B[*a*]P onto PA-6_42 and LDPE_215 ranged from 168–336 h and 120–168 h, respectively. For Anth sorption onto PA-6_42 and LDPE_215, the minimum equilibrium time ranged from 72–168 h (**Figure S5**). The recovery of the control samples ranged from 80–120% for Anth across low and high tested concentrations. Regarding B[*a*]P, the obtained recovery ranged from 86–97% across low and high tested concentrations. The analyte concentrations in the blank were below the limit of quantification of 2.5 µg/L.

The logarithmic sorption coefficients log $K_{MNP/w}$ derived by the batch-equilibrium and the TPP methods for the sorption of Anth and B[*a*]P to PA-6_42 and LDPE_215 are summarized in **Table S5.** The obtained log $K_{MNP/w}$ values are in good agreement. Also, according to Lee *et al.* [25], the reported log $K_{MNP/w}$ values of 4.77 and 7.17 for the sorption of Anth and B[*a*]P, respectively, to PE microplastics (median size: 420 µm) are within the same order of magnitude with the values obtained in this work using the TPP method.

Table S5: Comparison of the logarithmic sorption coefficient $K_{MNP/w}$ (L/kg) acquired applying the batch-equilibrium and TPP methods (n = 5 isotherm points in duplicate or triplicate, mean ± SD).

Sorbate	Sorbent	Batch	TPP
Anth	LDPE_215	4,57 ± 0,04	4,51 ± 0,09
	PA-6_42	4,93 ± 0,19	5,03 ± 0,06
B[a]P	LDPE_215	6,61 ± 0,04	6,58 ± 0,07
	PA-6_42	6,63 ± 0,05	6,82 ± 0,07

Similar to the TPP method, experimental sorption isotherms obtained using the batch-equilibrium method were fitted with the Langmuir model. The log of the Langmuir adsorption coefficient K_L (L/kg) describing the sorption of Anth to PA-6_42 and LDPE_215 were 4.96 and 4.73, respectively, while the obtained log of K_L for the sorption of B[*a*]P onto PA-6_42 and LDPE_215 were 6.65 and 6.60, respectively (**Figure S6**).

In comparison with the TPP method (**Table 2**), the difference between log K_L of the two methods for LDPE adsorption of Anth and B[*a*]P was within the standard error of the Langmuir model parameter K_L. Similarly, the difference between the K_L of the batch and TPP methods for PA-6_42 adsorption of Anth was well within the standard error of K_L. Of note, internal standard was spiked into the sample mixtures containing B[a]P and PA-6_42 after sorption equilibrium was reached in order to correct for nearly 50 % adsorption of B[a]P to the filter paper material. We attribute the slight deviation of the values for K_L to the sorption of fractions of the internal standard (B[*a*]P-d_{12}) to the PA-6 particles (potentially accompanied by displacement of some B[a]P) during the ca. 10 min filtration period. Overall, it can be concluded that the TPP method offers an easy, fast and reliable alternative for evaluating the adsorption properties of organic pollutants onto MNPs, circumventing these issues due to the lack of a filtration step.

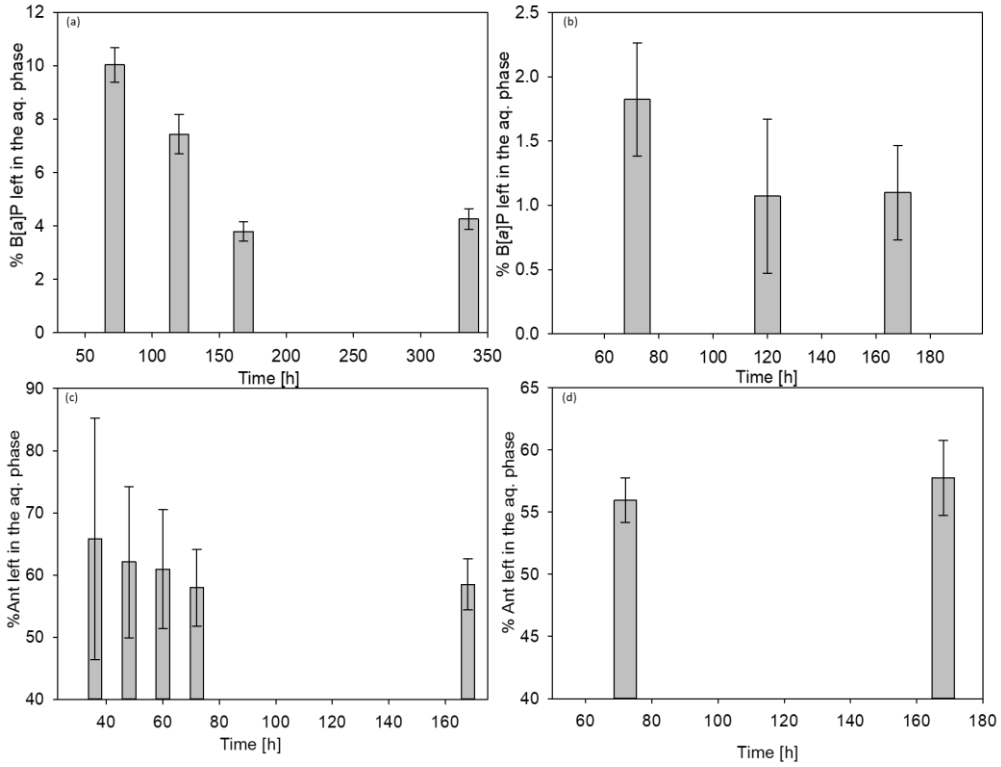

423

424 *Figure S5: Verification of equilibrium for the sorption of B[a]P on (a) PA-6, (b) LDPE, and Anth on (c)*
425 *PA-6 and (d) LDPE MNPs.*

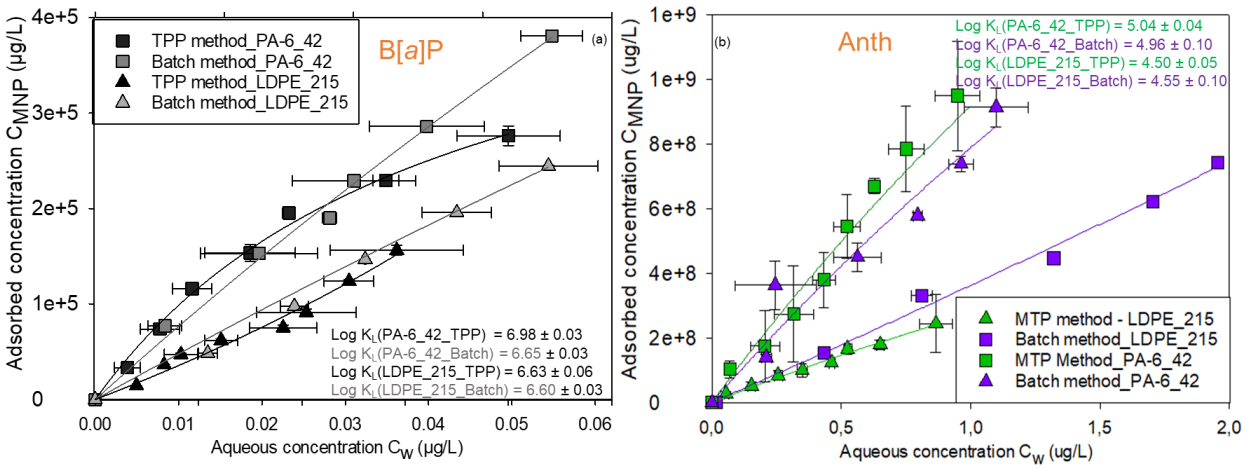

426

427 *Figure S6: Comparison of the Langmuir adsorption isotherms of (a) B[a]P and (b) Anth sorption to*
428 *LDPE_215 and PA-6_42 MNPs acquired with the TPP method and the batch-equilibrium method.*
429

Section S6: Experimentally Determined PAH Sorption Coefficients $K_{MNP/W}$ and Associated Combined Measurement Uncertainties

$K_{MNP/w}$ of PAH/MNP pairs and their respective combined measurement uncertainties u_c ($K_{MNP/w}$) are shown in **Table 6.** $K_{MNP/w}$ was calculated from the slopes within the linear range of each isotherm. The combined measurement uncertainty u_c ($K_{MNP/W}$) was calculated according to the ISO/IEC Guide to the Expression of Uncertainty in Measurement (GUM) [26]. Initially, the standard uncertainty of each component used to calculate $K_{MNP/w}$ (**Equation S14**) was determined.

$$K_{MNP/w} = \frac{1}{M_{MNP}}\left(\frac{K_{PDMS/w}}{C_{PDMS}} m_{total} - K_{PDMS} M_{PDMS} - V_w\right) \qquad \textbf{Equation S14 [11]}$$

u_c ($K_{MNP/W}$) was then calculated according to **Equation S15**,

$$u_{c=}\sqrt{\left[\frac{\partial y}{\partial M_{MNP}} * u(M_{MNP})\right]^2 + \left[\frac{\partial y}{\partial K_{PDMS/W}} * u\left(K_{PDMS/W}\right)\right]^2 + \left[\frac{\partial y}{\partial C_{PDMS}} * u(C_{PDMS})\right]^2 + \left[\frac{\partial y}{\partial m_{total}} * u(m_{total})\right]^2 + \left[\frac{\partial y}{\partial M_{PDMS}} * u(M_{PDMS})\right]^2 + \left[\frac{\partial y}{\partial V_W} * u(V_W)\right]^2} \qquad \textbf{Equation S15 [31]}$$

where y is the output quantity $K_{MNP/w}$.

The standard deviation of the measured $K_{PDMS/w}$ and C_{PDMS} were utilized as standard uncertainties u ($K_{PDMS/w}$) and u (C_{PDMS}), respectively. The relative standard uncertainty of the total amount of PAH spiked into the system u (m_{total}) was estimated as 5% (with 3.5% being the relative uncertainty of the analytical standard solution according to the manufacturers, and 1.5% being the relative uncertainty due to pipetting). The difference between the actual mass of MNPs M_{MNP} intended and the average mass weighted was utilized as the standard uncertainty of M_{MNP}. The systematic error due

to the weighing balance was ignored as negligible. The relative standard uncertainty resulting from measuring the volume of the aqueous phase was assigned to 1%. The uncertainty of the mass of PDMS in the coating of the stir bars, M_{PDMS}, was not declared by the producer and was therefore assigned to 1%.

The contribution of each component of $K_{MNP/w}$ to the combined uncertainty u_c was calculated according to **Equation S16**,

$$contribution\ (x_1) = \frac{\left[\frac{\partial y}{\partial x_1} * u(x_1)\right]^2}{\left[\frac{\partial y}{\partial x_1} * u(x_1)\right]^2 + \left[\frac{\partial y}{\partial x_2} * u(x_2)\right]^2 \ldots . + \left[\frac{\partial y}{\partial x_n} * u(x_n)\right]^2}$$

Equation S16 [26]

where x denote any of the six input components of $K_{MNP/w}$.

As shown in **Table S7**, u_c ($K_{MNP/w}$) was dominated by the standard uncertainties from $K_{PDMS/w,}$ followed by m_{total}, and $C_{PDMS.}$ For future applicability of this method, the contributions of the components to u_c ($K_{MNP/w}$) identify parameters that can be further optimized to reduce the uncertainty. Remarkably, the u_c ($K_{MNP/w}$) shown in **Table S6** are in the same order of magnitude as the model-generated standard error of K_L (**Table 2**).

Table S6: Experimentally determined sorption coefficients of PAHs onto MNPs obtained using the TPP method.

Polymer class	Polymer variants	Benzo[*a*]pyrene			Anthracene			Dibenzo[*a,l*]pyrene		
		$^{*}K_{MNP/w}$	$^{**}u_{c\,(k\,=\,1)}$	$^{'}$n	$^{*}K_{MNP/w}$	$^{**}u_{c\,(k\,=\,1)}$	$^{'}$n	$^{*}K_{MNP/w}$	$^{**}u_{c\,(k\,=\,1)}$	$^{'}$n
PMMA	PMMA_6	1.7E+05	6.3E+04	5						
	PMMA_0.3	3.6E+05	1.1E+05	5						
PU	PU_arom_1C	8.7E+05	3.0E+05	5						
	PU_arom_2C	3.5E+06	9.9E+05	5						
	PU_foam	1.6E+06	5.3E+05	5						
TPU	TPU_ester_Arom	1.4E+06	3.7E+05	5	1.7E+04	1.6E+04	3	9.7E+07	2.8E+07	5
	TPU_ether_Arom	2.0E+06	5.7E+05	5						
	TPU_ester_Alip	2.3E+06	6.1E+05	5						
	TPU_ether_Alip	2.5E+06	7.8E+05	5						
	TPU_ melt_arom	2.2E+06	7.0E+05	5						
PE	LDPE_215	2.5E+06	9.1E+05	5	3.62E+04	2.47E+04	5	5.4E+08	2.3E+08	5
	LDPE_84	8.0E+06	2.3E+06	5						
	PE_0.6	7.6E+06	1.9E+06	5						
PA	PA-6_42	3.3E+06	9.0E+05	5	1.0E+05	5.3E+04	8	5.7E+08	1.4E+08	5
	PA-12_44	5.3E+06	1.6E+06	5						
	PA-6_7	1.8E+07	5.3E+06	5						
Natural Rubber	Tire Rubber	2.0E+06	6.7E+05	5						
Aged polymers	Tire Rubber_1000h aged	2.0E+06	5.5E+05	4						
	Tire Rubber_2000h aged	1.9E+06	4.6E+05	4						
	PA-6_42_1000h aged	8.0E+06	2.1E+06	4						
	PA-6_42_2000h aged	5.0E+06	1.48E+06	4						
	LDPE_215_1000h aged	3.3E+06	9.3E+05	5						
	LDPE_215_2000h aged	3.2E+06	7.8E+05	4						

* Adsorption coefficient in (L/kg)

** Combined measurement uncertainty of $K_{MNP/w}$

' number of isotherms points used in duplicate or triplicate, and only points within the linear range of each isotherm were utilized to minimize bias.

Table S7: contributions of the uncertainty components of $K_{MNP/w}$ for the PAHs

		Contributions (Indexes) of the uncertainty components					
PAH	MNP	$K_{PDMS/W}$ (L/kg)	M_{mp} (kg)	M_{PDMS} (kg)	V_w (L)	C_{PDMS} (µg/kg)	m_{total} (ug)
B[a]P	PA-6_7	49.0%	3.2%	3.2%	3.2%	5.2%	36.2%
	PA-6_42	69.8%	0.0%	0.0%	0.0%	5.4%	24.9%
	PA-6_42_1000h	67.0%	0.0%	0.0%	0.0%	4.8%	28.1%
	PA-6_42_2000h	57.8%	0.0%	0.0%	0.0%	4.9%	37.2%
	PA-12_44	62.1%	0.0%	0.0%	0.0%	4.2%	33.7%
	PE_0.6	73.4%	0.0%	0.0%	0.0%	5.4%	21.2%
	LDPE_84	66.0%	0.0%	0.0%	0.0%	4.8%	29.1%
	LDPE_215	49.9%	0.0%	0.0%	0.0%	4.3%	45.7%
	LDPE_215_1000h	64.4%	0.0%	0.0%	0.0%	6.6%	29.0%
	LDPE_215_2000h	80.3%	0.0%	0.0%	0.0%	8.3%	11.4%
	Tire Rubber	50.2%	0.0%	0.0%	0.0%	6.1%	43.7%
	Tire Rubber_1000h	69.7%	0.0%	0.1%	0.0%	9.7%	20.6%
	Tire Rubber_2000h	85.2%	0.0%	0.1%	0.0%	10.6%	4.1%
	TPU_melt_arom	61.7%	0.0%	0.0%	0.0%	8.2%	30.1%
	TPU_ether_alip	57.1%	0.0%	0.0%	0.0%	6.9%	35.9%
	TPU_ether_arom	62.5%	0.0%	0.0%	0.0%	8.5%	28.9%
	TPU_ester_arom	79.7%	0.0%	0.1%	0.0%	13.9%	6.3%
	TPU_ester_alip	72.9%	0.0%	0.0%	0.0%	8.9%	18.1%
	PU_foam	56.3%	0.0%	0.1%	0.0%	9.2%	34.5%
	PU_arom_1C	51.2%	0.0%	0.2%	0.0%	15.5%	33.1%
	PU_arom_2C	65.9%	0.0%	0.0%	0.0%	6.5%	27.6%
	PMMA_0.3	61.3%	0.0%	0.1%	0.0%	13.3%	25.3%
	PMMA_6	52.8%	0.0%	0.5%	0.0%	26.3%	20.4%
Anth	PA-6_42	74.0%	0.0%	0.0%	0.0%	8.0%	17.9%
	LDPE_215	66.1%	0.0%	0.1%	0.1%	9.4%	24.5%
	TPU_ester_arom	81.7%	0.0%	0.1%	0.1%	12.8%	5.2%
DB[a,l]P	PA-6_42	76.4%	0.0%	0.0%	0.0%	6.1%	17.4%
	LDPE_215	34.9%	0.0%	0.0%	0.0%	3.1%	62.0%
	TPU_ester_arom	49.4%	0.0%	0.1%	0.0%	9.3%	41.2%

n = mean of at least nine isotherm points

Section S7: Evaluation of competitive sorption: sorption behavior of MNPs in single and tri-sorbate systems.

In order to understand possible competitive sorption effects, the sorption behavior of PA-6_42 and LDPE_215 MNPs were studied in mono-sorbate systems (containing a single specific PAH) and tri-sorbate systems (consisting of a mixture of the three PAHs

Anth, B[*a*]P and DB[*a,l*]P using similar concentration ranges, Fehler! Verweisquelle konnte nicht gefunden werden.**S7**). For both MNP types, a significant reduction in adsorption of Anth in the presence of the higher molecular weight PAHs was observed compared to mono-sorbate systems.

For B[*a*]P and PA-6_42, this effect was much less pronounced. In this case, the obtained K_L values were 17 and 30% lower in single-sorbate systems (B[*a*]P only) compared to tri-sorbate systems containing all three PAHs. The sorption of DB[*a,l*]P was unaffected or even slightly enhanced by the presence of Anth and B[*a*]P. It appears that for a mixture of PAHs, the sorption of the higher molecular weight and more hydrophobic PAHs are more favorable, while the smaller and least hydrophobic PAHs such as Anth suffer from competition for available sorption sites. This suggest a hydrophobicity-driven antagonism and is in line with the findings of Baker *et al*. (2012) [27].

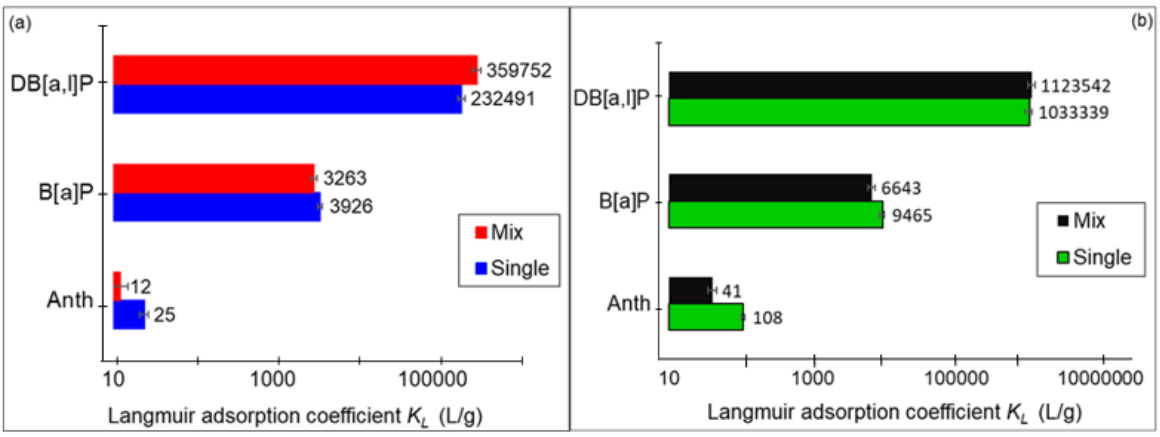

Figure S7: Langmuir adsorption coefficient K_L for Anth, B[a]P and DB[a,l]P sorption on (a) LDPE_215 and (b) PA-6_42 MNPs in single and tri-sorbate systems (error bars represent the standard errors, note that the x-axes are expressed in logarithmic scale).

References SI

1. Prieto, A., et al., *Stir-bar sorptive extraction: A view on method optimisation, novel applications, limitations and potential solutions.* J Chromatogr A, 2010. **1217**(16): p. 2642-66.
2. Mayer, P., et al., *Equilibrium sampling devices.* Environ Sci Technol, 2003. **37**(9): p. 184A-191A.
3. Prieto, A., et al., *Development of a stir bar sorptive extraction and thermal desorption-gas chromatography-mass spectrometry method for the simultaneous determination of several persistent organic pollutants in water samples.* J Chromatogr A, 2007. **1174**(1-2): p. 40-9.
4. Gorecki, T. and J. Pawliszyn, *Effect of sample volume on quantitative analysis by solid-phase microextraction. Part 1. Theoretical considerations.* Analyst, 1997. **122**(10): p. 1079-86.
5. Kot-Wasik, A., D. Dąbrowska, and J. Namieśnik, *Photodegradation and biodegradation study of benzo(a)pyrene in different liquid media.* Journal of Photochemistry and Photobiology A: Chemistry, 2004. **168**(1-2): p. 109-115.
6. May, W.E., et al., *Solution thermodynamics of some slightly soluble hydrocarbons in water.* Journal of Chemical & Engineering Data, 2002. **28**(2): p. 197-200.
7. Barco-Bonilla, N., et al., *Comprehensive analysis of polycyclic aromatic hydrocarbons in wastewater using stir bar sorptive extraction and gas chromatography coupled to tandem mass spectrometry.* Anal Chim Acta, 2011. **693**(1-2): p. 62-71.
8. Baltussen, E., et al., *Study into the Equilibrium Mechanism between Water and Poly(dimethylsiloxane) for Very Apolar Solutes: Adsorption or Sorption?* Analytical Chemistry, 1999. **71**(22): p. 5213-5216.
9. Grant, S., et al., *Experimental Solubility Approach to Determine PDMS-Water Partition Constants and PDMS Activity Coefficients.* Environ Sci Technol, 2016. **50**(6): p. 3047-54.
10. DiFilippo, E.L. and R.P. Eganhouse, *Assessment of PDMS-water partition coefficients: implications for passive environmental sampling of hydrophobic organic compounds.* Environ Sci Technol, 2010. **44**(18): p. 6917-25.
11. Jonker, M.T.O. and A.A. Koelmans, *Polyoxymethylene solid phase extraction as a partitioning method for hydrophobic organic chemicals in sediment and soot.* Environmental Science & Technology, 2001. **35**(18): p. 3742-3748.
12. Mayer, P., W.H. Vaes, and J.L. Hermens, *Absorption of hydrophobic compounds into the poly(dimethylsiloxane) coating of solid-phase microextraction fibers: high partition coefficients and fluorescence microscopy images.* Anal Chem, 2000. **72**(3): p. 459-64.

13. Ayawei, N., A.N. Ebelegi, and D. Wankasi, *Modelling and Interpretation of Adsorption Isotherms.* Journal of Chemistry, 2017. **2017**: p. 1-11.
14. Gunay, A., E. Arslankaya, and I. Tosun, *Lead removal from aqueous solution by natural and pretreated clinoptilolite: adsorption equilibrium and kinetics.* J Hazard Mater, 2007. **146**(1-2): p. 362-71.
15. Batool, F., et al., *Study of Isothermal, Kinetic, and Thermodynamic Parameters for Adsorption of Cadmium: An Overview of Linear and Nonlinear Approach and Error Analysis.* Bioinorg Chem Appl, 2018. **2018**: p. 3463724.
16. Gupta, S. and A. Kumar, *Removal of nickel (II) from aqueous solution by biosorption on A. barbadensis Miller waste leaves powder.* Applied Water Science, 2019. **9**(4).
17. Lončarski, M., et al., *Sorption behavior of polycyclic aromatic hydrocarbons on biodegradable polylactic acid and various nondegradable microplastics: Model fitting and mechanism analysis.* Science of The Total Environment, 2021. **785**.
18. Aharoni, C. and M. Ungarish, *Kinetics of activated chemisorption. Part 2.—Theoretical models.* Journal of the Chemical Society, Faraday Transactions 1: Physical Chemistry in Condensed Phases, 1977. **73**(0).
19. Foo, K.Y. and B.H. Hameed, *Insights into the modeling of adsorption isotherm systems.* Chemical Engineering Journal, 2010. **156**(1): p. 2-10.
20. Staudt, P.B., et al., *A new method for predicting sorption isotherms at different temperatures using the BET model.* Journal of Food Engineering, 2013. **114**(1): p. 139-145.
21. Ebadi, A., J.S. Soltan Mohammadzadeh, and A. Khudiev, *What is the correct form of BET isotherm for modeling liquid phase adsorption?* Adsorption, 2009. **15**(1): p. 65-73.
22. Demirbas, E., M. Kobya, and A.E.S. Konukman, *Error analysis of equilibrium studies for the almond shell activated carbon adsorption of Cr(VI) from aqueous solutions.* Journal of Hazardous Materials, 2008. **154**(1-3): p. 787-794.
23. Belhachemi, M. and F. Addoun, *Comparative adsorption isotherms and modeling of methylene blue onto activated carbons.* Applied Water Science, 2011. **1**(3-4): p. 111-117.
24. *OECD Guideline for the testing of chemicals: Adsorption - Desorption Using a Batch Equilibrium Method*. 2000.
25. Lee, H., W.J. Shim, and J.H. Kwon, *Sorption capacity of plastic debris for hydrophobic organic chemicals.* Sci Total Environ, 2014. **470-471**: p. 1545-52.
26. ISO/IEC, *Uncertainty of measurement — Part 3: Guide to the expression of uncertainty in measurement (GUM:1995)*. 2008. p. 120.

27. Bakir, A., S.J. Rowland, and R.C. Thompson, *Competitive sorption of persistent organic pollutants onto microplastics in the marine environment.* Mar Pollut Bull, 2012. **64**(12): p. 2782-9.